OPTIMAL SYNTHESIS OF LINE SOURCE ANTENNAS BASED ON RHODES DISTRIBUTIONS

J. C. Brégains, J. A. Rodríguez, F. Ares and E. Moreno

Grupo de Sistemas Radiantes, Departamento de Física Aplicada,

Facultad de Física, Universidad de Santiago de Compostela.

15782 - Santiago de Compostela – Spain

faares@usc.es

ABSTRACT

In this paper we show that by means of an appropriate optimization technique the zeros of Rhodes radiation patterns can be perturbed so as to improve or modify pattern and/or the aperture distribution characteristics without altering the behaviour of the excitation amplitude distribution at the ends of the aperture. The examples presented include symmetric and asymmetric shaped beams, sum patterns with individually controlled side lobe heights, shaped beams generated by real excitations, and sum pattern aperture distributions that are smoother than the original Rhodes distribution.

1. INTRODUCTION

The standard distribution solutions to the problem of minimizing the beam width of a line source sum pattern given a specified maximum side lobe level *SLL* are the Taylor family [1]

$$h_T(\zeta) = \frac{1}{2a} \sum_{m=-(\bar{n}-1)}^{\bar{n}-1} F_T(m) \exp(-jm\pi\zeta / a) \tag{1}$$

where $2a$ is the length of the aperture, ζ is the distance from its centre, $\bar{n}$ is an integer parameter ($\bar{n}$ -1 is the number of controlled side lobes on each side of the main beam, the heights of which are close to *SLL*), and F_T is the radiation pattern. F_T is given by

$$F_T(u) = \frac{\sin \pi u}{\pi u} \frac{\prod_{n=1}^{\bar{n}-1} \left(1 - \frac{u^2}{(u_T)_n^2}\right)}{\prod_{n=1}^{\bar{n}-1} \left(1 - \frac{u^2}{n^2}\right)} \tag{2}$$

where $u = (2a/\lambda)\cos\theta$ (θ being the angle from broadside) and

$$(u_T)_n = \bar{n} \left[\frac{A^2 + (n - \frac{1}{2})^2}{A^2 + (\bar{n} - \frac{1}{2})^2} \right]^{1/2} \tag{3}$$

the parameter A being related to *SLL* by $A = (1/\pi)\cosh^{-1}(10^{SLL/20})$.

Rhodes [2] pointed out that Taylor was wrong in assuming it to be physically possible for the line source amplitude to behave as a non-zero constant at the edges of the aperture. Rhodes showed that the amplitude of the tangential electric field component perpendicular to the aperture edge must in fact be proportional to distance from the edge, and that the parallel component must go to zero quadratically as it approaches the edge. The upshot of this correction for low-sidelobe sum patterns is the Rhodes family of distributions:

$$h_R(\zeta) = \sum_{m=-(\bar{n}-1)}^{\bar{n}-1} F_R(m+\tfrac{1}{2}) \exp(-j[m+\tfrac{1}{2}]\pi\zeta / a) \tag{4}$$

where

$$F_R(u) = \frac{\cos \pi u}{1-4u^2} \frac{\prod_{n=1}^{\bar{n}-1}\left(1-\dfrac{u^2}{(u_R)_n^2}\right)}{\prod_{n=1}^{\bar{n}-1}\left(1-\dfrac{u^2}{\left(n+\frac{1}{2}\right)^2}\right)} \tag{5}$$

with

$$(u_R)_n = (\bar{n}+\tfrac{1}{2})\left[\frac{A^2+(n-\frac{1}{2})^2}{A^2+(\bar{n}-\frac{1}{2})^2}\right]^{1/2} \tag{6}$$

Compared with the Taylor distribution for the same values of A and $\bar{n}$, the Rhodes sum pattern has a slightly broader main beam; allows the use of larger values of $\bar{n}$ without incurring in superdirectivity; and, for $u > \bar{n}$, has a slightly steeper side lobe taper. The amplitude of the Rhodes aperture distribution goes to zero linearly at the ends of the antenna, but the slope is steep and preceded by a sharp rise, so that the edge-brightening problem of Taylor distributions is not significantly ameliorated.

In previous papers, Elliott [3] and ourselves [4-7] have shown that patterns other than conventional symmetric sum patterns can be achieved by using Taylor sum patterns as the starting points of appropriate optimization procedures. Specifically, the papers cited perturbed the zeros of F_T to achieve sum patterns with side lobes of individually arbitrary heights [3]; symmetric [4] and asymmetric [5] shaped beams; real aperture distributions affording shaped beams [5,6]; and aperture distributions with no edge-brightening affording sum patterns, difference patterns or shaped beams [7]. Here we report that application of the same approach to Rhodes distributions can achieve similar results without significantly altering the behaviour of the Rhodes distribution at the edges of the aperture.

2. METHOD

To achieve *a*) shaped beams (which requires the radiation pattern to have complex zeros) and *b*) control over different numbers of side lobes on either side of the main beam, it is necessary to generalize eq. (5): numbering the zeros of $(\cos \pi u)/(1\text{-}4u^2)$ consecutively from 1 up on each side of the main beam,

$$F(u) = \frac{\cos \pi u}{1-4u^2} \frac{\prod_{n\in\Omega_l}\left(1-\frac{u}{u_{l,n}+jv_{l,n}}\right)\prod_{n\in\Omega_r}\left(1-\frac{u}{u_{r,n}+jv_{r,n}}\right)\prod_{n\in\Xi_l}\left(1-\frac{u}{u_{l,n}}\right)\prod_{n\in\Xi_r}\left(1-\frac{u}{u_{r,n}}\right)}{\prod_{n\in\Omega_l\cup\Xi_l}\left(1+\frac{u}{\left(n+\frac{1}{2}\right)}\right)\prod_{n\in\Omega_r\cup\Xi_r}\left(1-\frac{u}{\left(n+\frac{1}{2}\right)}\right)} \qquad (7)$$

where $\Omega_l \subset \mathbf{N}$ and $\Omega_r \subset \mathbf{N}$ contain the indices of filled nulls on respectively the left and right of the main beam, and $\Xi_l \subset \mathbf{N}$ and $\Xi_r \subset \mathbf{N}$ the indices of unfilled but shifted nulls on respectively the left and right of the main beam. The aperture distribution $h(\zeta)$ is given by eq. (4) with $h(\zeta)$ instead of $h_R(\zeta)$ and $F(m+½)$ instead of $F_R(m+½)$. In each specific application, the optimal values of the shifted zeros $u_{l,n}+jv_{l,n}$ and $u_{r,n}+jv_{r,n}$ (where $v_{l,n} = 0$ and $v_{r,n} = 0$ for unfilled nulls) are found by successive perturbations using an appropriate optimization technique to minimize a cost function C that penalizes the deviation of pattern and/or aperture distribution parameters from desired values.

3. EXAMPLES

In this section we exemplify the potential of the above approach by synthesizing excitation distributions complying with a variety of pattern or aperture distribution requirements. All these examples concern a line source of length $2a = 10\lambda$, and in all cases the optimization technique employed was simulated annealing [8].

3.1. Symmetric sum patterns with unequal controlled side lobes.

If we seek a symmetric sum pattern in which the heights of the first seven side lobes on each side of the main beam are to be given by

$$SLL_{1,\mathrm{d}} = SLL_{2,\mathrm{d}} = SLL_{3,\mathrm{d}} = \text{-}40 \text{ dB}$$

$SLL_{4,d} = SLL_{5,d} = SLL_{6,d} = SLL_{7,d} = -20$ dB

where $SLL_{i,d}$ is the desired height of the i-th side lobe, then in eq. (7) we make $\Omega_l = \Omega_r = \varnothing$, $\Xi_l = \Xi_r = \{1,2,3,4,5,6,7\}$ and $u_{l,n} = -u_{r,n}$, and we optimize a cost function

$$C = \sum_{i=1}^{7} (SLL_i - SLL_{i,d})^2 \tag{8}$$

The pattern so obtained is shown in Fig.1, and its nulls $u_{r,n}$ are listed in Table 1; its peak directivity is 15.23. The excitation amplitude distribution is shown in Fig. 2 (the phase is of course zero for this symmetric pattern). Note that, as expected, the amplitude approaches the end of the aperture linearly, but that the edge-brightening peak at the end of the distribution makes the distribution very irregular. The amelioration of this undesirable behaviour is discussed in Section 3.6 below.

3.2. Symmetric flat-topped beams with controlled side lobes.

If we wish to obtain a symmetric flat-topped beam by filling the first two nulls on either side of the main beam, and at the same time ensure that the first three side lobes have desired levels $SLL_{i,d}$, then in eq. (7) we make $\Omega_l = \Omega_r = \{1,2\}$, $\Xi_l = \Xi_r = \{3,4,5\}$, $u_{l,n} = -u_{r,n}$ and $v_{l,n} = -v_{r,n}$, and we optimize the cost function

$$C = \sum_{i=1}^{5} (SLL_i - SLL_{i,d})^2 + \sum_{i=1}^{2} (Z_i - Z_{i,d})^2 \tag{9}$$

where $SLL_{1,d} = SLL_{2,d} = 0$, Z_i is the power level at filled null i (i.e. at $u = u_{r,i}$ or $u = u_{l,i}$ (i = 1,2)), and $Z_{i,d}$ is the desired deviation from the beam peak level at this point. For $Z_{1,d} = Z_{2,d} = -1$ dB and $SLL_{3,d} = SLL_{4,d} = SLL_{5,d} = -20$ dB, the pattern and distribution results are shown in Figs.3-5 and the values of the $u_{r,n}$ and $v_{r,n}$ are listed in Table 2.

3.3. Symmetric flat-topped beams with controlled side lobes generated by real excitations.

To achieve null filling with a real excitation distribution it is necessary for each of the complex zeros of $F(u)$ to be accompanied by its complex conjugate. We therefore

set $\Omega_l = \Omega_r = \{1,2,3,4\}$, $\Xi_l = \Xi_r = \{5,6,7\}$, $u_{l,n} = -u_{r,n}$, $v_{l,n} = -v_{r,n}$, $u_{r,2} = u_{r,1}$, $u_{r,4} = u_{r,3}$, $v_{r,2} = -v_{r,1}$ and $v_{r,4} = -v_{r,3}$. For the same desired side lobe and ripple levels as in Section 3.2, the results obtained with an appropriately modified version of eq. (9) as cost function are shown in Figs.6 and 7 and the $u_{r,n}$ and $v_{r,n}$ are listed in Table 3. The price paid for ensuring that excitation distribution is real by making consecutive filled zeros mutual conjugates is a significant broadening of the main beam.

3.4. Asymmetric sum patterns.

To obtain a sum pattern with desired inner side lobe levels $SLL_{r,i,\mathrm{d}} = -25\,\mathrm{dB}$ on the right of the main beam and $SLL_{l,i,\mathrm{d}} = -15\,\mathrm{dB}$ on the left, we set $\Omega_l = \Omega_r = \varnothing$ and $\Xi_l = \Xi_r = \{1,2,3,4,5,6,7\}$ without symmetry constrains relating the $u_{l,n}$ and $u_{r,n}$. For the cost function, instead of eq.8, we use

$$C = \sum_{i=1}^{7}(SLL_{l,i} - SLL_{l,i,d})^2 + \sum_{i=1}^{7}(SLL_{r,i} - SLL_{r,i,d})^2 \qquad (10)$$

The results are shown in Figs.8-10 and the $u_{l,n}$ and $u_{r,n}$ are listed in Table 4. Note that, as for all asymmetric radiation patterns without any filled nulls, the amplitude of the excitation distribution is symmetric and its phase antisymmetric. The amplitude and phase distributions are in fact both quite similar to those obtained by Elliott [3] starting from a Taylor distribution, particularly as regards the edge-brightening peaks being the global amplitude maxima for the whole aperture; apart from the behaviour of the amplitude at the ends of the aperture, the main difference between Elliott's amplitude distribution and that of Fig.9 is that the latter has greater amplitudes than the former at the centre of the aperture.

3.5. A cosec-squared pattern with asymmetric controlled side lobes.

We wish to obtain a cosec-squared pattern with at most $\pm 1\,\mathrm{dB}$ of ripple by filling the first two nulls on the right of the main beam, and at the same time to limit the first three side lobes on the right of the shaped beam to $-25\,\mathrm{dB}$ and the first three on the left to $-20\,\mathrm{dB}$. We therefore set $\Omega_l = \varnothing$, $\Omega_r = \{1,2\}$, $\Xi_l = \{1,2,3\}$ and $\Xi_r = \{3,4,5\}$, and we

use the cost function

$$C = \sum_{i=1}^{3}(SLL_{l,i} - SLL_{l,i,d})^2 + \sum_{i=1}^{5}(SLL_{r,i} - SLL_{r,i,d})^2 + \sum_{i=1}^{2}(Z_i - Z_{i,d})^2 \qquad (11)$$

with

$SLL_{r,1,\mathrm{d}}$ = -5 dB, $SLL_{r,2,\mathrm{d}}$ = -10 dB; $Z_{1,\mathrm{d}}$ = -6 dB, $Z_{2,\mathrm{d}}$ = -11 dB;

$SLL_{r,3,\mathrm{d}} = SLL_{r,4,\mathrm{d}} = SLL_{r,5,\mathrm{d}}$ = -25 dB; and

$SLL_{l,1,\mathrm{d}} = SLL_{l,2,\mathrm{d}} = SLL_{l,3,\mathrm{d}}$ = -20 dB

The results are presented in Figs.11-13 and Table 5.

3.6. Symmetric sum patterns generated by smooth aperture distributions.

A pattern that satisfies the same specifications as for the pattern of Section 3.1 can be achieved using a smoother aperture distribution than in Section 3.1 if null-filling is allowed ($\Omega_l = \Omega_r = \{1,2,3,4,5,6,7\}$, $\Xi_l = \Xi_r = \varnothing$, $u_{l,n} = -u_{r,n}$, $v_{l,n} = -v_{r,n}$) and the cost function of eq. (8) is supplemented with *a*) a term Z preventing the levels of the filled nulls from rising above the adjacent side lobe levels, *b*) a term V limiting the local variation of the excitation amplitude distribution:

$$C = c_1\sum_{i=1}^{7}(SLL_i - SLL_{i,d})^2 + c_2 Z + c_3(V - V_d)^2 \qquad (12)$$

where for desired maximum null filling levels $Z_{i,\mathrm{d}}$,

$$Z = \sum_{i=1}^{q}(Z_i - Z_{i,d})^2 \qquad (13)$$

with $q = 4$ if $Z_i < Z_{i,\mathrm{d}}$ for $4 < i < 7$ and $q = 7$ otherwise; $V = \max\{R_j\}$, where R_j is the difference between the j-th peak of the excitation amplitude distribution and the lower of its flanking minima; V_d is the desired value of V; and the c_i are adjustable constants controlling the relative importance of fixing side lobe levels, null-filling levels, and the local and global variation of the excitation amplitude distribution. Note that the null-filling term always restrains the first three null-filling levels but allows the outer four nulls to be filled to levels below the specified level.

The radiation pattern and aperture distribution obtained for the same $SLL_{i,d}$ as in Section 3.1, $Z_{1,d} = Z_{2,d} = Z_{3,d} = Z_{4,d} = -41$ dB, $Z_{5,d} = Z_{6,d} = Z_{7,d} = -25$ dB, and $V_d = 0.1$ are shown as continuous curves in Figs. 14-16 (with the corresponding functions of Section 3.1 shown as dashed curves for comparison), and the $u_{r,n}$ and $v_{r,n}$ are listed in Table 6. The operational price paid for this improvement is just a 3.48% reduction in directivity.

3.7. Rhodes patterns without edge-brightening.

Finally, we apply our methodology to making the aperture distributions for Rhodes patterns smoother without raising the side lobe levels of the patterns themselves or significantly reducing their peak directivities. For a Rhodes pattern with $\bar{n} = 9$ and a side lobe level of -20 dB ($\Omega_l = \Omega_r = \varnothing$, $\Xi_l = \Xi_r = \{1,2,3,4,5,6,7,8\}$, $u_{l,n} = -u_{r,n}$, $v_{l,n} = v_{r,n} = 0$, $SLL_{i,d} = -20$ dB), we use the cost function

$$C = c_1 \sum_{i=1}^{8} \Delta_i^2 H(\Delta_i) + c_2 (D - D_d)^2 + c_3 (V - V_d)^2 \qquad (14)$$

where D is the peak directivity of the pattern, D_d its desired value (that of the original Rhodes pattern, in this case 18.92), $\Delta_i = (SLL_i - SLL_{i,d})$ and H is the Heaviside step function. The continuous curves in Figs.17 and 18 show the results obtained for $V_d = 0.1$, and the dashed curves those of the original Rhodes distribution. Note that edge-brightening has been totally eliminated, the price paid being a slight (1.3%) reduction in peak directivity (now 18.67). The values of the $u_{r,n}$ are listed for both patterns in Table 7.

4. FINAL REMARKS

The above examples show that by means of an appropriate optimization technique the zeros of Rhodes radiation patterns can be perturbed so as to improve or modify pattern and/or the aperture distribution characteristics without altering the linear behaviour of the excitation amplitude distribution at the ends of the aperture. In this way it is possible to achieve symmetric and asymmetric shaped beams, sum patterns with individually

controlled side lobe heights, and sum pattern aperture distributions that are smoother than the original Rhodes distribution. The syntheses presented here, in which optimization was performed by simulated annealing, took between 10 seconds and 3 minutes on a PC with an AMD-K6-2 processor running at 500 MHz. For the examples of Sections 3.1-3.5 Orchard's deterministic optimization method [9] is even faster, converging in just two or three iterations, but Orchard's method cannot deal with the problems of Sections 3.6 and 3.7. Finally, it may be pointed out that sampling of the aperture distribution allows the present results to be applied to linear array antennas; and that if this is done then, the resulting linear array can be further optimized by using optimization techniques appropriate to discrete arrays.

ACKNOWLEDGEMENTS

This work was supported by the Xunta de Galicia under project PGIDT00PXI20603PR.

REFERENCES

[1] Taylor, T. T., "Design of line-source antennas for narrow beam width and low side lobes", *IRE Trans. Antenna Propagat.*, Vol. AP-3, pp. 16-28, 1955.

[2] Rhodes, D. R., "On the Taylor distribution", *IEEE Trans. Antennas Propagat.*, Vol. AP-20, No. 2, pp. 143-145, 1972.

[3] Elliott, R. S., "Design of line-source antennas for sum patterns with side lobes of individually arbitrary heights", *IEEE Trans. Antennas Propagat.*, Vol. AP-24, pp. 76-83, 1976.

[4] Ares, F., R. S. Elliott, and E. Moreno, "Optimised synthesis of shaped line-source antenna beams", *Electronics Letters*, Vol. 29, No. 12, pp. 1136-1137, 1993.

[5] Ares, F., and J. A. Rodríguez, "Asymmetric-shaped beam patterns from a continuous linear aperture distribution", *Microwave Opt. Technol. Lett.*, Vol. 15, No. 5, pp. 288-291, 1997.

[6] Ares, F., R. S. Elliott, and E. Moreno, “Synthesis of shaped line-source antenna beams using pure real distributions”, *Electronics Letters*, Vol. 30, No. 4, pp. 280-281, 1994.

[7] Ares, F., and J. A. Rodríguez, “Smooth, efficient real amplitude distributions with no edge brightening for linear and circular near-Taylor sum patterns”, *Electronics Letters*, Vol. 34. No. 7, pp.611-612, 1998.

[8] Press, W.H., S. A. Teukolsky, W. T. Vetterling, and B. P. Flannery, *Numerical Recipes in C*, 2nd Edition, Cambridge University Press, pp. 444-455, 1992.

[9] Orchard, H.J., R. S. Elliott, and G. D. Stern, “Optimising the synthesis of shaped beam antenna patterns”, *IEE Proc. Pt. H.*, Vol. 132, pp. 63-68, 1985.

LEGENDS FOR FIGURES AND TABLES

Fig.1. Symmetric sum pattern obtained in Section 3.1.

Fig.2. Amplitude of the aperture distribution affording the radiation pattern of Fig.1.

Fig.3. Flat-topped beam obtained in Section 3.2. Ripple, $\pm$ 0.5 dB; side lobe level, -20 dB.

Fig.4. Amplitude of the aperture distribution affording the radiation pattern of Fig.3.

Fig.5. Phase of the aperture distribution affording the radiation pattern of Fig.3.

Fig.6. Flat-topped beam obtained in Section 3.3 using a real aperture distribution. Ripple, $\pm$ 0.5 dB; side lobe level, -20 dB.

Fig.7. Amplitude of the aperture distribution affording the radiation pattern of Fig.6.

Fig.8. Asymmetric sum pattern obtained in Section 3.4. Side lobe levels, -15 and -25 dB.

Fig.9. Amplitude of the aperture distribution affording the radiation pattern of Fig.8.

Fig.10. Phase of the aperture distribution affording the radiation pattern of Fig.8.

Fig.11. Cosec-squared pattern obtained in Section 3.5. Ripple, $\pm$ 1 dB; side lobe levels, -20 and -25 dB.

Fig.12. Amplitude of the aperture distribution affording the radiation pattern of Fig.11.

Fig.13. Phase of the aperture distribution affording the radiation pattern of Fig.11.

Fig.14. Symmetric sum pattern obtained in Section 3.6 while minimizing the variation (——), and the pattern obtained in Section 3.1 without aperture optimization (- - - - - - -).

Fig.15. Amplitudes of the aperture distributions affording the radiation patterns of Fig.14. Note the reduction in edge-brightening.

Fig.16. Phase of the aperture distribution affording the radiation pattern of Fig.14.

Fig.17. Symmetric sum pattern similar to a Rhodes pattern obtained with a smooth aperture distribution in Section 3.7 (——), and the original -20 dB $\bar{n} = 9$ Rhodes pattern used as starting point.

Fig.18. Amplitudes of the aperture distributions affording the radiation patterns of Fig.17. Note the reduction in edge-brightening.

Table 1. Zeros of the radiation pattern of Fig.1 (Section 3.1).

Table 2. Zeros of the radiation pattern of Fig.3 (Section 3.2).

Table 3. Zeros of the radiation pattern of Fig.6 (Section 3.3).

Table 4. Zeros of the radiation pattern of Fig.8 (Section 3.4).

Table 5. Zeros of the radiation pattern of Fig.11 (Section 3.5).

Table 6. Zeros of the radiation pattern of Fig.14 (Section 3.6).

Table 7. Zeros of the radiation patterns of Fig.17 (Section 3.7).

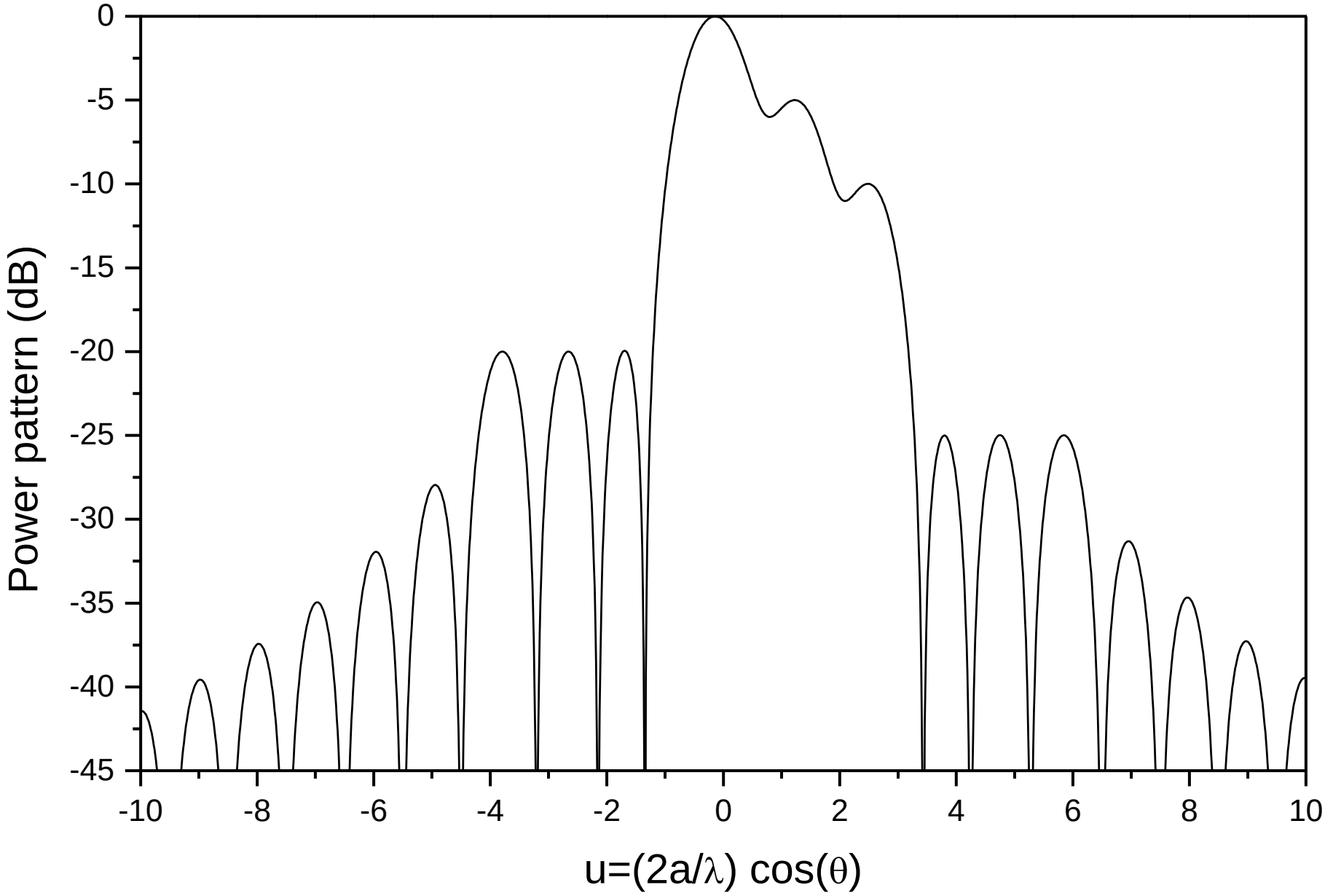
0
-5
-10
-15
-20
-25
-30
-35
-40
-45
Power pattern (dB)
-10
-8
-6
-4
-2
0
2
4
6
8
10
u=(2a/λ) cos(θ)

Fig.1

Fig.80

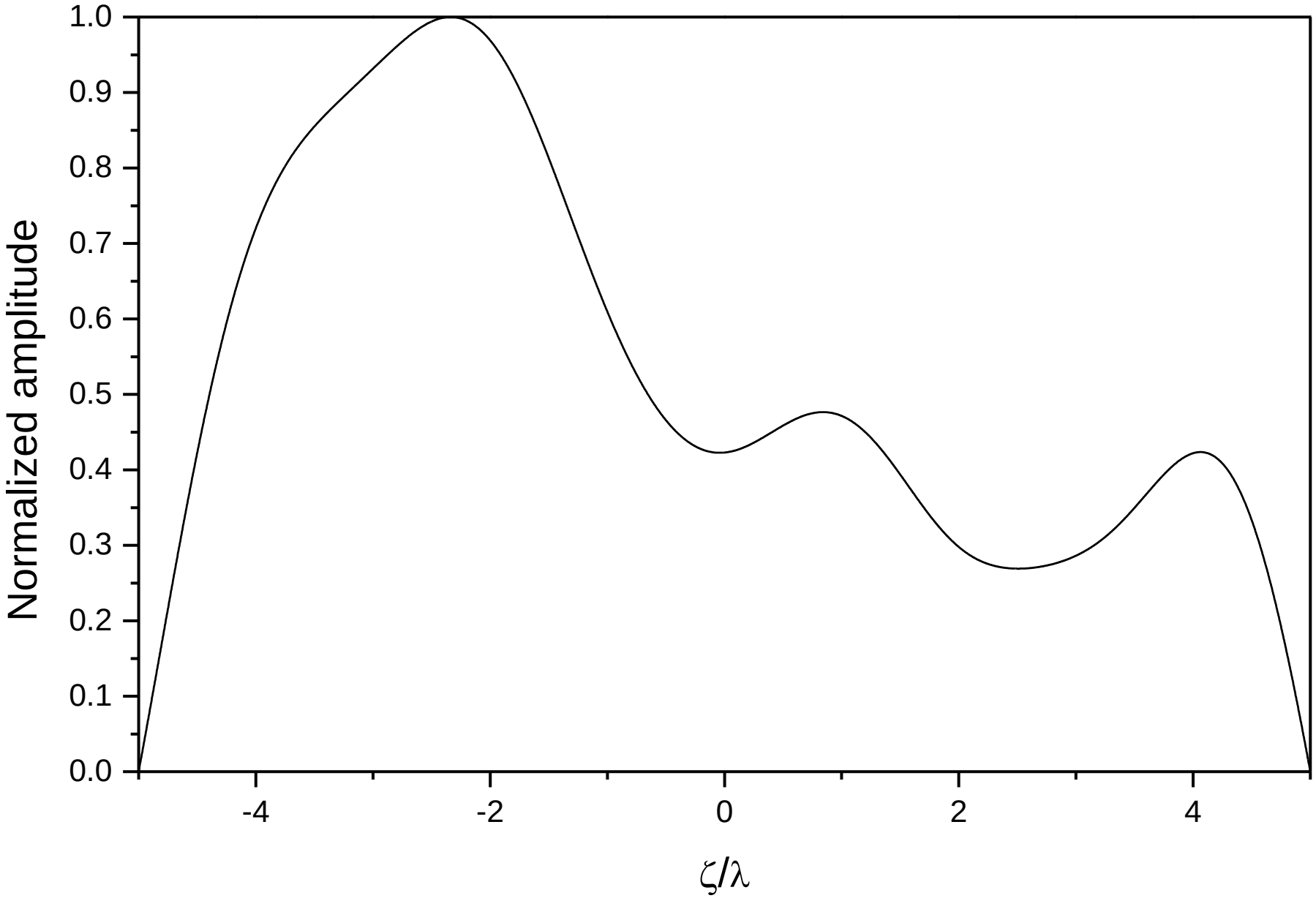

Fig.12

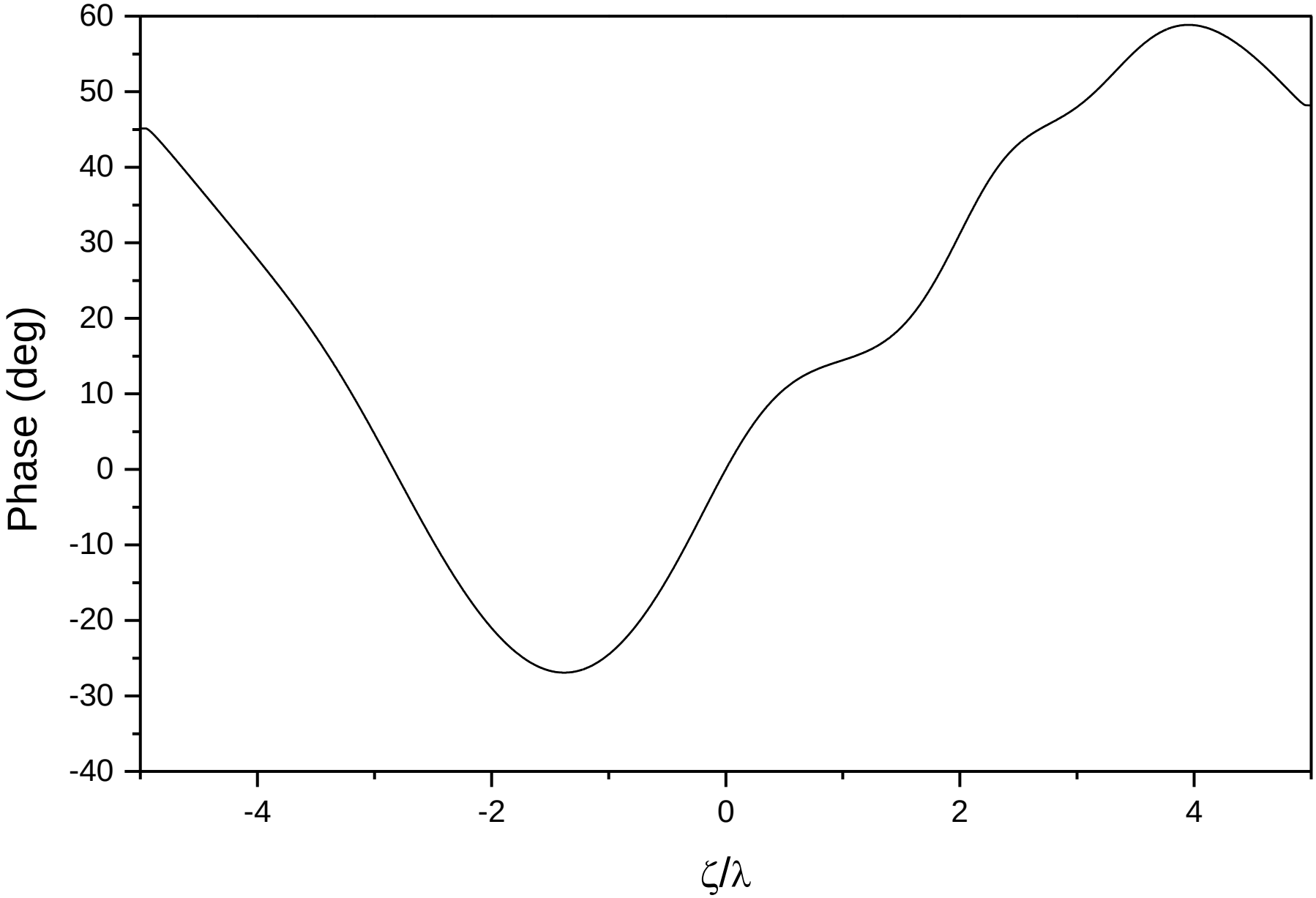

Fig.13

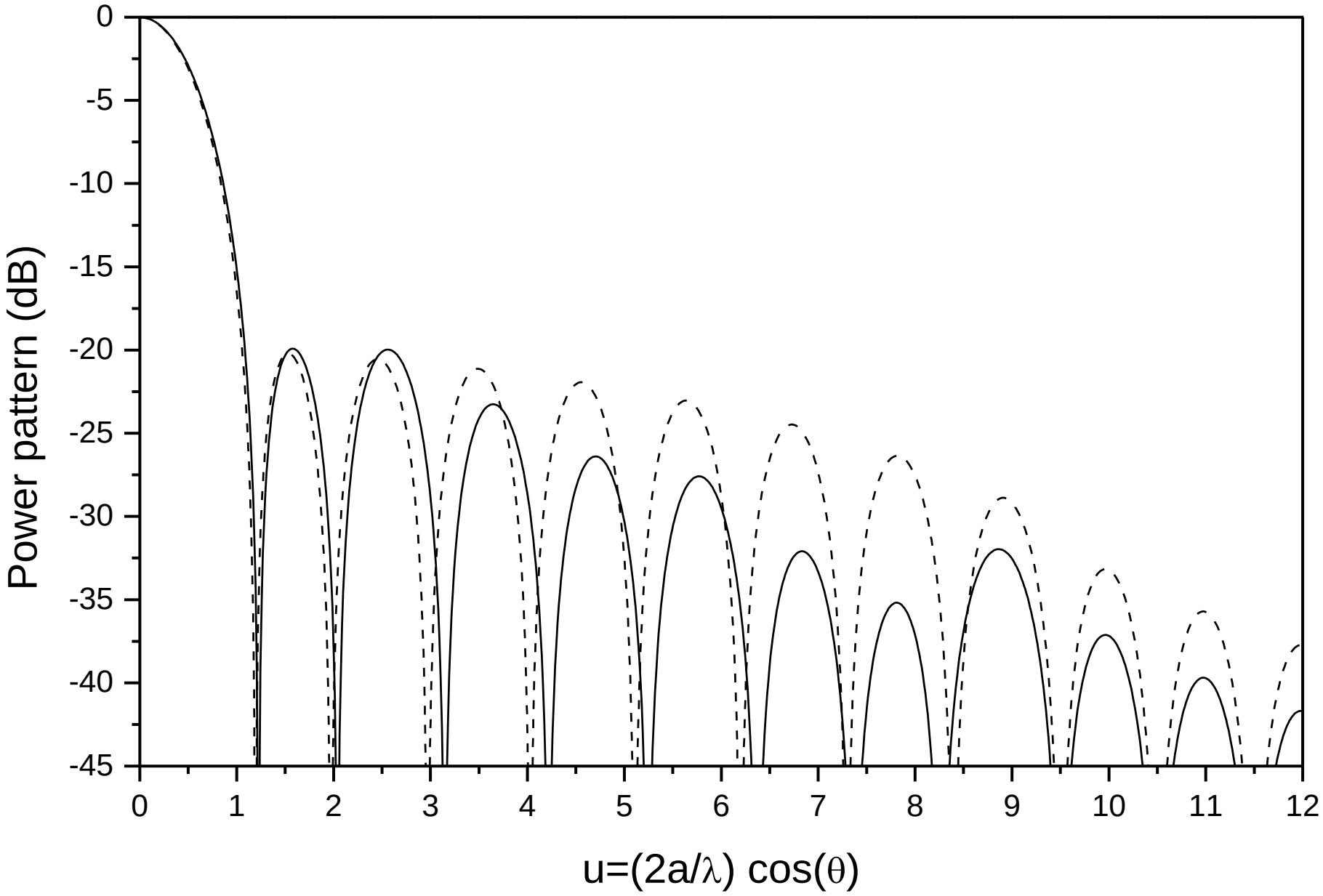
0
-5
-10
-15
-20
-25
-30
-35
-40
-45
Power pattern (dB)
0
1
2
3
4
5
6
7
8
9
10
11
12
u=(2a/λ) cos(θ)

Fig.16

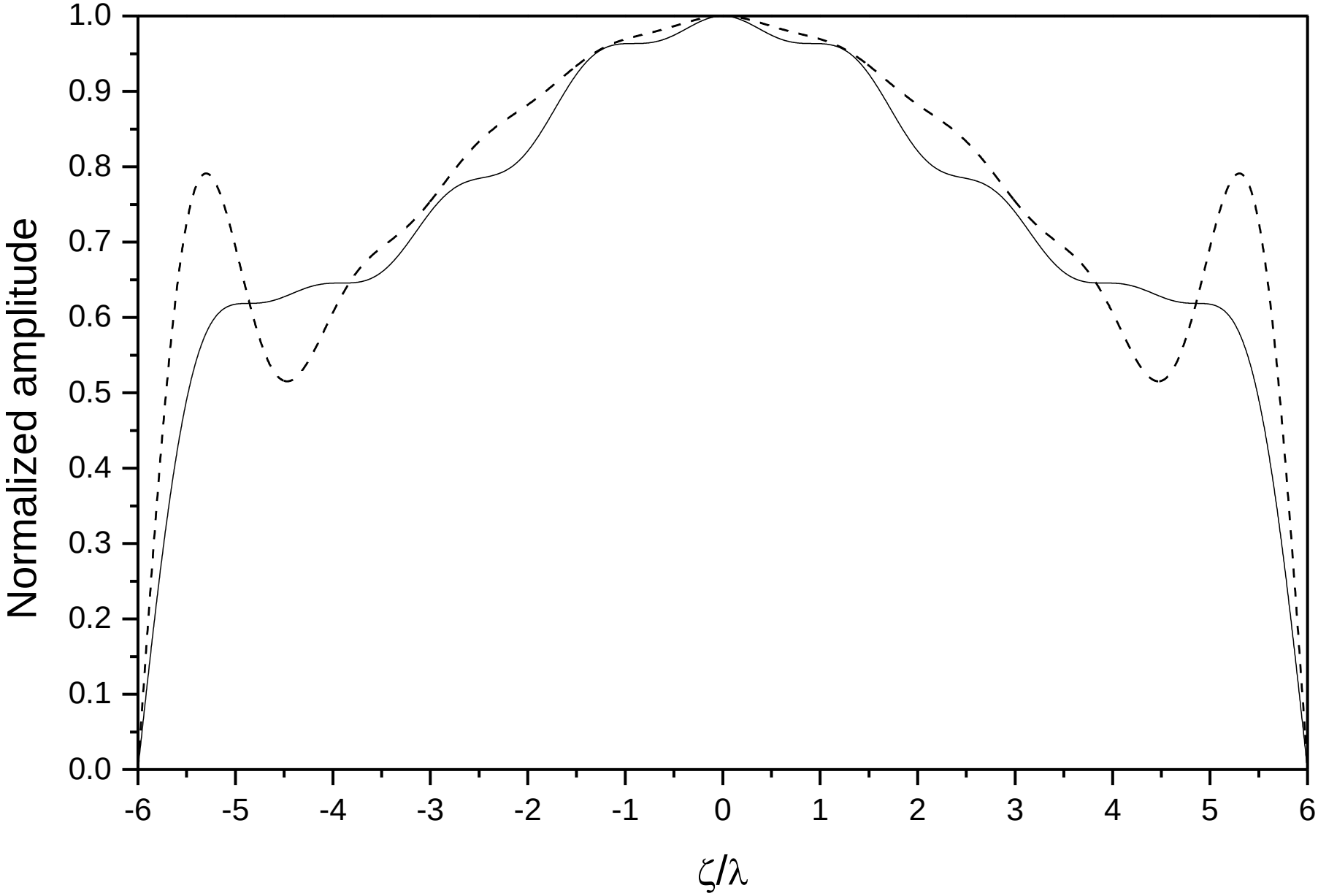
Normalized amplitude
1.0
0.9
0.8
0.7
0.6
0.5
0.4
0.3
0.2
0.1
0.0
-6
-5
-4
-3
-2
-1
0
1
2
3
4
5
6
ζ/λ

Fig.18

n	$u_{r,n}$
1	1.653
2	2.106
3	2.749
4	3.308
5	4.791
6	5.964
7	7.142

Table 1

n	$u_{r,n}$	$v_{r,n}$
1	0.591	-0.537
2	1.776	0.532
3	3.532	0.000
4	4.297	0.000
5	5.305	0.000

Table 2

n	$u_{r,n}$	$v_{r,n}$
1	1.025	1.148
2	3.053	1.080
3	5.312	0.000
4	7.223	0.000
5	6.156	0.000

Table 3

n	$u_{r,n}$	$u_{l,n}$
1	1.560	-0.755
2	2.223	-1.626
3	3.131	-2.668
4	4.115	-3.754
5	5.143	-4.857
6	6.198	-5.980
7	7.286	-7.144

Table 4

n	$u_{r,n}$	$v_{r,n}$	$u_{l,n}$	$v_{l,n}$
1	0.721	-0.378	-1.346	0.000
2	2.019	-0.345	-2.147	0.000
3	3.433	0.000	-3.203	0.000
4	4.248	0.000	--	--
5	5.279	0.000	--	--

Table 5

n	$u_{r,n}$	$v_{r,n}$
1	1.754	0.101
2	2.155	0.233
3	2.724	0.259
4	3.224	0.139
5	4.777	0.215
6	5.930	0.219
7	7.109	0.059

Table 6

	$u_{r,n}$	
	Rodhes	**Optimised**
n	u_n	u_n
1	1.195	1.226
2	1.974	2.040
3	2.972	3.148
4	4.029	4.218
5	5.109	5.244
6	6.200	6.370
7	7.297	7.365
8	8.397	8.267

Table 7